Behaviour at high pressure of $(Cs,K)Al_4Be_5B_{11}O_{28}$ (londonite): an *in situ* single-crystal synchrotron diffraction study up to 26 GPa

Running title: Elastic behaviour of londonite

Abstract

Introduction

Experimental methods

Results: Elastic behaviour

Results: Pressure-induced structure evolution

Discussion and Conclusions

Acknowledgements

References

Tables and Figures

Corresponding author: Paolo LOTTI
Dipartimento di Scienze della Terra,
Università degli Studi di Milano,
Via Botticelli 23,
I-20133 Milano,
Italy
Email: paolo.lotti@unimi.it
Tel. : +39 02 503 15607
Fax: +39 02 503 15597

Manuscript submitted to Journal of American Ceramic Society

Behaviour at high pressure of $(Cs,K)Al_4Be_5B_{11}O_{28}$ (londonite): an *in situ* single-crystal synchrotron diffraction study up to 26 GPa

G. Diego Gatta[1,2], Paolo Lotti[1], Davide Comboni[1], Marco Merlini[1], Pietro Vignola[3], Hanns-Peter Liermann[4]

[1] Dipartimento di Scienze della Terra, Università degli Studi di Milano, Via Botticelli 23, I-20133 Milano, Italy
[2] CNR - Istituto di Cristallografia, Via G. Amendola 122/o, I-70126 Bari, Italy
[3] CNR-Istituto per la Dinamica dei Processi Ambientali, Via M. Bianco 9, I-20131 Milano, Italy
[4] DESY, HASYLAB, PETRA III, Notkestr. 85, D-22607 Hamburg, Germany

Abstract

The compressional behaviour and the *P*-induced deformation mechanisms at the atomic scale of $(Cs,K)Al_4Be_5B_{11}O_{28}$ (londonite, a~7.31 Å and space group $P\bar{4}3m$) were investigated by *in-situ* single-crystal synchrotron X-ray diffraction with a diamond anvil cell up to 26 GPa. No phase transition was observed within the *P*-range investigated: this material remains elastically isotropic (*i.e.*, with cubic symmetry) in response to the applied pressure. Fitting the *P*-*V* data with a Birch-Murnaghan isothermal equation of state, we obtained: V_0 = 390.8(3) Å^3, K_{P0}= 212(7) GPa ($\beta_0 = 1/K_{P0}$ = 0.0047(1) GPa^{-1}) and K'= 4.6(6). A series of structural refinements, based on the high-pressure intensity data, were performed. The stiffness of londonite (similar to that of carbides) is governed by its close-packing structure, and in particular by the very low compressibility of B- and Be-tetrahedra and the modest compressibility of the Al-octahedra. The Cs-polyhedra are the most compressible units of the structure. The effects of pressure can be accommodated by intra-polyhedral compression or deformation, leading to a modest bulk compression. The high amount of boron in londonite (B_2O_3~50wt%) makes its synthetic counterpart a potential neutron absorber. In addition, the high content of Cs makes londonite-type materials as potential hosts for nuclear waste.

Keywords: londonite, high pressure, compressibility, structure refinements, neutron absorber materials.

Introduction

Londonite is a rare Cs-bearing mineral with ideal chemical formula $(Cs,K)Al_4Be_4(B,Be)_{12}O_{28}$ (with Cs > K[1]). The K-dominant analogue is rhodizite. The real chemical composition of londonite-rhodizite has been a matter of debate for about a century (as reviewed by Gatta et al. [2]). The crystal structure of rhodizite-londonite was solved and refined by Taxer and Buerger[3], by single-crystal X-ray diffraction, with a = 7.318(1) Å and space group $P\bar{4}3m$ and ideal chemical formula $CsAl_4Be_4B_{12}O_{28}$. Later, Pring et al.[4] reinvestigated the crystal chemistry and the crystal structure of a K-dominant rhodizite, confirming the structure model of Taxer and Buerger[3]. More recently, Gatta et al.[2] reinvestigated the crystal chemistry of a londonite from the granitic pegmatites of the Antsongombato Gem Mine, Betafo district, Madagascar, by means of wavelength dispersive X-ray spectroscopy (EPMA-WDS), laser-ablation inductively coupled plasma-mass spectroscopy (LA-ICP-MAS), inductively coupled plasma atomic emission spectroscopy (ICP-AES), and single-crystal neutron diffraction at 300 and 20 K. The structure model was found to be consistent with that previously reported by Taxer and Buerger[3] and Pring et al.[4], giving new insights into the B- and Be-distribution in the structure. The building block units of the structure of londonite-rhodizite are represented by clusters of four edge-sharing Al-octahedra (with Al at a 4*e* site, $x \sim 0.361$), linked to B- and Be-tetrahedra (12*h* site at $x \sim 0.248$ and 4*e* site at $x \sim 0.258$, respectively) with a configuration like that shown in Fig. 1. The alkali cations (*i.e.*, Cs, Rb, K) lie at the unit-cell origin and occupy cavities of approximately tetrahedral geometry with coordination number CN=12 (1*a* site, $x = 0$). Pekov et al.[5] described the londonite-rhodizite structure as built from: a sub-framework of BO_4-

tetrahedra, $[B_{12}O_{24}]_{\infty\infty\infty}$, topologically identical to the $[Al_6Si_6O_{24}]_{\infty\infty\infty}$ framework in sodalite, and clusters of four octahedra sharing edges, building units of the pharmacosiderite structure. The combination of these composite units, $[M_4O_4]$ and $[T_{12}O_{24}]$ (*M*: octahedron, *T*: tetrahedron), found in the pharmacosiderite and sodalite structures, results in the complex composite unit $[Al_4O_4B_{12}O_{24}]$ of londonite structure. However, in this structure description the Be^{2+} (along with the alkali cations) are considered to fill the interstices and compensate for its anionic charge. The neutron structural refinements and the chemical analyses of Gatta et al.[2] suggested that: the tetrahedral 4*e* site (at $x \sim 0.258$) is mainly occupied by Be, but a low amount of B (~3%) likely occurs; the tetrahedral 12*h* site (at $x \sim 0.248$) is mainly occupied by B, but a significant fraction of Be (~12%) is present[2]. On the basis of the chemical analyses (by EPMA-WDS, LA-ICP-MAS, and ICP-AES) and of the cation partitioning derived by the neutron structure refinement, the structural formula of londonite (on the basis of 28 oxygen atoms per formula unit) was given[2] as:

$^{1a}(Cs_{0.36}K_{0.34}Rb_{0.15}Ca_{0.04}Na_{0.02})_{\Sigma 0.91}{}^{4e}(Al_{3.82}Li_{0.05}Fe_{0.02})_{\Sigma 3.89}{}^{4e}(Be_{3.82}B_{0.18})_{\Sigma 4}$

$^{12h}(B_{10.97}Be_{1.00}Si_{0.01})_{\Sigma 11.98}O_{28}$.

Gatta et al.[6] investigated the stability and the thermo-elastic behaviour of the londonite previously studied by Gatta et al.[2] up to 1273(3) K (at 0.0001 GPa) and up to 4.85(5) GPa (at 298 K) by means of *in-situ* synchrotron X-ray powder diffraction. No evidence of phase transition or anomalous thermo-elastic behaviour was observed up to 973 K. At $T > 973$ K, londonite shows the first evidence of a structure destabilization. The volume thermal expansion coefficient between 298 and 973 K, obtained by linear regression, was: $\alpha_0 = 1/V\cdot(\partial V/\partial T)_{P0,T0} = 2.38(6)\cdot 10^{-5}\ K^{-1}$. Londonite showed a fully elastic behaviour up to 4.85 GPa and no phase transition was observed within the pressure-range investigated. *P*-*V* data fitted to a second-order Birch-Murnaghan isothermal equation of state gave: $V_0 = 389.1(1)\text{Å}^3$ and $K_{P0} = 1/\beta_0 = V\cdot(\partial P/\partial V)_{P0} = 280(12)$ GPa. A so high bulk modulus value was

not predictable, as it approaches those of carbides (*e.g.*, B_4C with K_{P0} ~ 245-306 GPa[7,8]). The modest *P*-range investigated (for a so stiff material) and the absence of structural data (*i.e.*, only the unit-cell parameters were obtained by Le Bail full-profile fitting[9]) did not allow a deep description of the *P*-induced elastic behaviour and the main deformation mechanisms at the atomic scale[6]. As a result, the reasons of an almost uncompressible behaviour of londonite are still obscure. Considering the good thermo-elastic behaviour (substantiated by the significantly low-compressibility and the modest thermal expansion up to 1000 K) and the significantly high fraction of boron (B_2O_3 ~50 wt%), the synthetic counterparts of londonite could be considered as potential inorganic host for ^{10}B in composite neutron-absorbing materials. In this light, the aim of this study is an extension of the previous, and preliminary, investigation on the compressional behaviour of londonite by *in-situ* single-crystal synchrotron X-ray diffraction experiment with a diamond anvil cell to a pressure in excess of 25 GPa.

Experimental methods

For the high-pressure (H*P*) experiment of this study, we used fragments of the same gem-quality sample of londonite (from the granitic pegmatites of the Antsongombato Gem Mine, Betafo district, Madagascar) previously used by Gatta et al.[2,6]. A preliminary check of crystals was performed using a KUMA-KM4 X-ray four-circle diffractometer (Mo*K*α radiation) at the Earth Science Department University of Milano. The high-pressure synchrotron X-ray single-crystal diffraction experiment was conducted at the Extreme Conditions Beamline P02.2 at PETRA-III/DESY, Hamburg, Germany[10]. Data collections were performed with an incident beam of 42.7 keV in energy (λ = 0.2904 Å), and a focusing spot of ~8.5 (H) μm x 1.8 (V) μm originated from a compound refractive lenses system, consisting of 121 Be lenses with a radius of 50 μm (400 μm beam acceptance) and a focal

length of 1221 mm. A single crystal of londonite (~40 x 30 x 25 μm^3) was selected for the synchrotron experiment. The crystal was loaded in a symmetric DAC equipped with Boehler-Almax design diamonds/seats with a 70° opening and 300 μm culets size. A 250 μm thick rhenium gasket was pre-indented to 50 μm and then drilled with 200 μm hole, in which the crystal of londonite and some ruby microspheres for pressure determination (by ruby-fluorescence method[11]) were located. Neon was used as hydrostatic pressure-transmitting medium[12]. Pressure was increased with an automated pressure-driven membrane system and measured with the online ruby/alignment system. Diffraction data were successfully collected up to ~26 GPa; data sets were also collected in decompression (Table 1), in order to prove the reversibility of the *P*-induced deformation mechanisms. Diffraction patterns were acquired on a PerkinElmer XRD 1621 flat panel detector, using an in-house script for collecting step-scan diffraction images. Sample to detector distance was calibrated using a CeO_2 standard (NIST 674a). The data collection strategy consisted in a pure ω-scan (-30°≤ ω ≤ +30°), with a step size of 1° and an exposure time of 1 s/frame. The diffraction images were then converted to conform to the "Esperanto" format of the program CrysAlis[13,14]. Bragg peaks were indexed and their intensities were integrated and corrected for Lorentz-polarization effects, using the CrysAlis package[13]. Scaling and correction for absorption (due to the DAC components) was applied by the semi-empirical *ABSPACK* routine implemented in CrysAlis. The refined unit-cell parameters at different pressures are listed in Table 1. No evidence of phase transitions was observed within the *P*-range investigated; all the diffraction patterns were successfully indexed in the $P\bar{4}3m$ space group.

The structure refinements, based on the data collected at high pressure, were performed in the acentric space group $P\bar{4}3m$ using the SHELXL-97 software[15,16], starting from the structure model of Gatta et al.[2]. The neutral X-ray scattering curve of Cs, Al, Be, B and O were used to model the site population. The secondary isotropic extinction effect was first

corrected according to Larson's protocol[17], as implemented in the SHELXL-97 package[15,16], however its contribute was found to be negligible for all the data sets. Due to the limitations of the H*P*-data sets, the structure refinements were conducted with atomic isotropic displacement parameters and assigning: 1) Al to the octahedral 4*e* site (at $x \sim 0.361$; full site occupancy, fixed), 2) Be to the tetrahedral 4*e* site (at $x \sim 0.258$, full site occupancy, fixed), 3) B to the tetrahedral 12*h* site (at $x \sim 0.248$, full site occupancy, fixed), and Cs to the 1*a* site (at $x = 0$, partial site occupancy, refined). The refined partial site occupancy of the 1*a* site, here modelled with the scattering curve of Cs alone, reflects the actual multi-elements population of Cs, Rb and K, as reported by Gatta et al.[2].

With such a configuration, convergence was rapidly achieved and the variance-covariance matrix showed no significant correlation among the refined parameters for all the data sets. At the end of the last cycle of refinements, no peak larger than +0.4/-0.4 e^-/Å^3 was present in the final difference-Fourier map of the electron density (CIFs deposited). The final agreement indexes were all with $R_1(F) < 3\%$ for 17 refined parameters and (at least) 70 unique reflections with $Fo > 4\sigma(Fo)$ (CIFs deposited). Atomic coordinates, site occupancy factors and thermal displacement parameters are deposited as CIFs. Relevant bond lengths and angles are listed in Table 2.

Results: Elastic behaviour

The evolution of the unit-cell volume of londonite with pressure (data listed in Table 1) is shown in Fig. 2. The compressional pattern appears to be monotonic, without any evidence of phase transition or change of the compressional behavior. Data collected in decompression prove a fully elastic behavior within the *P*-range investigated.

Unit-cell volumes *vs.* *P* were fitted to a Murnaghan (M-EoS)[18] and to a third-order Birch-Murnaghan Equation of State (III-BM-EoS)[19] using the EOS-FIT5.2 program[20]. These two isothermal equations of state are widely used in order to describe the compressional behavior of crystalline materials in low/middle *P*-regimes (see Angel[21] for a review), and allow to refine the isothermal bulk modulus of a given material K_{P0} [$K_{P0} = V \cdot (\partial P/\partial V)_{P0}$, which is the reciprocal of the thermodynamic volume compressibility coefficient $\beta_0 = 1/K_{P0} = 1/V \cdot (\partial V/\partial P)_{P0}$], and its *P*-derivatives ($K' = \partial K_{P0}/\partial P$, $K'' = \partial^2 K_{P0}/\partial P^2$). The simplest EoS is that proposed by Murnaghan[18], based on the assumption that the isothermal bulk modulus varies linearly with pressure, and takes the form:

$$P = (K_{P0}/K')[(V_{P0}/V_P)^{K'} - 1],$$

where V_{P0} and V_P represent the unit-cell volume (or molar volume) at ambient and H*P* conditions, respectively. The Birch-Murnaghan EoS[19] is based upon the assumption that the high-pressure strain energy in a solid can be expressed as a Taylor series in the Eulerian finite strain, defined as:

$$f_E = [(V_{P0}/V_P)^{2/3} - 1] / 2.$$

Expansion in the Eulerian strain polynomial has the following form:

$$P(f_E) = 3K_{P0} f_E (1 + 2 f_E)^{5/2} \{1 + 3/2(K' - 4) f_E + 3/2[K_{P0}K'' + (K' - 4)(K' - 3) + 35/9] f_E^2 + \ldots\}.$$

For the experimental data of londonite, the fit was performed using the data weighted by the uncertainties in *P* and *V*. The refined elastic parameters are: $V_0 = 390.8(3)$ Å ^{3}, $K_{P0} = 213(6)$ GPa and $K' = 4.3(5)$ for a M-EoS fit and $V_0 = 390.8(3)$Å^3, $K_{P0} = 212(7)$ GPa and $K' = 4.6(6)$ for a III-BM-EoS fit, respectively. As shown by the statistical fit parameters and by the maximum difference between observed-calculated *P* values, the fit quality of the two EoS is identical (with $w\chi^2 = 2.5$ and $\Delta P_{max} = -0.5$ GPa).

The confidence-ellipses referred to the 68.3%, 95.4% and 99.7% confidence-levels, respectively ($\Delta\chi^2 = 2.30$, $\pm 1\sigma$; $\Delta\chi^2 = 6.17$, $\pm 2\sigma$; $\Delta\chi^2 = 11.8$, $\pm 3\sigma$), were then calculated using

the variance-covariance matrices of K_{P0} and K' obtained from the least-squares procedure for the III-BM-EoS fit[21]. The ellipses are elongated with negative slope (Fig. 2), showing a negative correlation of the parameters K_{P0} and K'. Considering a 99.7% confidence-level, the elastic parameters are: K_{P0} = 212 ± 13 GPa and K' = 4.6 ± 1.0.

The evolution of the Eulerian finite strain *vs.* "normalized stress" ($Fe = P/[3fe(1+2fe)^{5/2}]$) plot (*i.e.*, *fe-Fe* plot[21]) is shown in Fig. 2. The intercept value obtained by a weighted linear regression through the data points is $Fe(0)$ = 211(2) GPa, and the slope of the regression line leads to a K' value of 4.5(2), in good agreement with the elastic parameters obtained by the III-BM-EoS fit.

Results: Pressure-induced structure evolution

The structural evolution with P, at the atomic scale, can be better described on the basis of the compression and deformation mechanisms of the building units of londonite structure: the Be- and B-tetrahedron, the Al-octahedron and the Cs-polyhedron.

The Be-tetrahedron shows an anisotropic compression in response to the applied pressure, with the Be-O1 (x1) length almost constant and the Be-O3 (x3) length monotonically compressed with P (Fig. 3, Table 2). However, the two independent On-Be-On angles [*i.e.*, O3-Be-O3 (x3) and O3-Be-O1 (x3)] appear to keep their original values with P (within 2σ), suggesting no angular deformation within the P-range investigated.

A different behaviour is observed for the B-tetrahedron. The two independent bond distances [*i.e.*, B-O2 (x2) and B-O3 (x2)] show a similar compressional trend with P (Fig. 3, Table 2). The four independent tetrahedral angles behave differently: O2-B-O2 (x1) and O3-B-O3 (x1) show almost constant values with increasing P, whereas O2-B-O3' (x2) increases and O2-B-O3 (x2) decreases with P (Fig. 3, Table 2). Despite the almost isotropic compression of the B-tetrahedron, as deduced on the basis of the similar B-O2 and B-O3

shortening, the different behaviour of the On-B-On angles suggests a slight distortion with *P* (maximum variation of the On-B-On angles of about 2°).

The Al-octahedron is stiff but more compressible than Be- or B-tetrahedra, and the large Cs-polyhedron is the most compressible unit of the structure. The *P*-induced shortening of the two independent Al-On bond lengths [*i.e.*, Al-O1 (x3) and Al-O2 (x3)] is similar and significant within the *P*-range investigated (about 0.05-0.06 Å, Fig. 3, Table 2). The shortening of the only independent Cs-O3 length (x 12) is the most pronounced one (about 0.17 Å, Fig. 3, Table 2).

Discussion and Conclusions

The experimental findings of this study show that londonite preserves its crystallinity at least up to 26 GPa, and behaves elastically under hydrostatic compression. No phase transition is observed within the *P*-range investigated, and this is a valuable result: this material remains elastically isotropic (*i.e.*, with cubic symmetry) in response to the applied pressure. The preliminary data obtained by Gatta et al.[6] showed that londonite behaves like an (almost) uncompressible material. However, the bulk modulus obtained by Gatta et al.[6] exploring a modest *P*-range (*i.e.*, K_{P0} = 280(12) GPa, P_{max} = 5 GPa) was overestimated. Overall, the stiffness of londonite is confirmed in this study: its bulk modulus (K_{P0} = 212(7) GPa) is drastically higher than that of several B/Al-bearing ceramic materials (*e.g.*, boron-mullite Al_5BO_9 with K_{P0} ~ 165 GPa[22,23] 2:1 mullite, with adiabatic bulk modulus K_s ~ 169 GPa[24]), toward those of carbides (*e.g.*, B_4C with K_{P0} ~ 245–306 GPa[7,8]). The refined value of the bulk modulus *P*-derivatives (*i.e.*, *K'* = 4.6(6)) is in line with that expected for crystalline materials[19].

The stiffness of londonite is governed by its close-packing structure and bonding topology, and in particular by the very low compressibility of B- and Be-tetrahedra and the

modest compressibility of the Al-octahedra, which represent the principal building-block units of the londonite structure. The Cs-polyhedra are the most compressible units of the structure. The closed-packing structure hinders a compression through the inter-polyhedral tilting, usually observed in framework compounds as the energetically less-costly mechanism[e.g.25-27]. The effects of pressure can therefore be accommodated mainly by intra-polyhedral compression or deformation, leading to a modest bulk compression of the structure.

Londonite-type compounds can be of technological interest. The high amount of boron in londonite (B_2O_3 ~50wt%) makes its synthetic counterpart a potential neutron absorber, due to the high capacity of boron to absorb neutrons [the absorption cross section of boron of 'normal' isotopic constitution, *i.e.* ^{10}B 20% + ^{11}B 80%, is 749 ± 4 barns at 2,200 m/s, whereas it is 3,835 ± 9 barns for pure ^{10}B] [28,29]. Neutron absorber materials usually consist of alloy or composite materials that contain a neutron absorber nuclide, and are used, for example, in spent fuel applications (in order to maintain the fuel in a subcritical condition[30]), or in medical applications (*e.g.*, neutron capture therapy for cancer[31]). The high content of Cs and Rb (CsO_2 + RbO_2 ≥ 8 wt%) makes londonite-type materials as potential host for nuclear waste.

As highlighted by Gatta et al.[6], the thermal instability of londonite at T > 1,000 K could be considered a weak point for the applications of this material. However, at T < 1000 K this compound shows a modest thermal expansion coefficient. Combining the elastic parameters obtained in this study and the thermal data of Gatta et al.[6], a *P*-*T*-*V* equation of state of londonite, valid at a first approximation up to 26 GPa and 1,000 K, can be obtained:

$$V_{(P,T)} \sim V_{(P0,T0)}[1 - \beta_0 \Delta P + \alpha_0 \Delta T] = V_{(P0,T0)}[1 - 0.0047(1)\cdot \Delta P + 2.38(6)\cdot 10^{-5}\cdot \Delta T]$$

(with $\beta_0 = 1/K_{P0}$ in GPa^{-1} and α_0 in K^{-1}).

Acknowledgements

Parts of this research were carried out at the light source PETRA III at DESY, a member of the Helmholtz Association (HGF).

References

[1]W. B. Simmons, F. Pezzotta, A. U. Falster and K. L. Webber, "Londonite, a new mineral species: The Cs-dominant analogue of rhodizite from the Antandrokomby granitic pegmatite, Madagascar", *Can. Mineral.*, **39,** 747–755 (2001).

[2]G. D. Gatta, P. Vignola, G. J. McIntyre and V. Diella, "On the crystal chemistry of londonite [(Cs,K,Rb)$Al_4Be_5B_{11}O_{28}$]: a single-crystal neutron diffraction study at 300 and 20 K", *Am. Mineral.*, **95,** 1467-1472 (2010).

[3]K. J. Taxer and M. J. Buerger, "The crystal struture of rhodizite", *Z. Kristallogr.*, **125,** 423-436 (1967).

[4]A. Pring, V. K. Din, D. A. Jefferson and J. M. Thomas, "The crystal chemistry of rhodizite: a re-examination", *Mineral. Mag.*, **50,** 163-172 (1986).

[5]I. V. Pekov, O. V. Yakubovich, W. Massa, N. V. Chukanov, N. N. Kononkova, A. A. Agakhanov and V. Y. Karpenko, "Londonite from the Urals, and new aspects of the crystal chemistry of the rhodizite- londonite series", *Can. Mineral.*, **48**, 241-254 (2010).

[6]G. D. Gatta, P. Vignola and Y. Lee, "Stability of (Cs,K)$Al_4Be_5B_{11}O_{28}$ (londonite) at high pressure and high temperature: a potential neutron absorber material", *Phys. Chem. Minerals*, **38,** 429-434 (2011).

[7]R. Lazzari, N. Vast, J. M. Besson, S. Baroni, A. Dal Corso, "Atomic structure and vibrational properties of icosahedral B_4C boron carbide", *Phys. Rev. Lett.*, **83,** 3230–3233 (1999).

[8]T. Fujii, Y. Mori, H. Hyodo and K. Kimura, "X-ray diffraction study of B_4C under high pressure", *J. Phys. Conf. Ser.*, **215,** 012011 (doi:10.1088/1742-6596/215/1/012011) (2010).

[9]A. Le Bail, H. Duroy and J. L. Fourquet, "Ab-initio structure determination of $LiSbWO_6$ by X-ray powder diffraction", *Mat. Res. Bull.*, **23,** 447-452 (1988).

[10]H-P. Liermann, Z. Konôpková, W. Morgenroth, K. Glazyrin, J. Bednarčik, E. E. McBride, S. Petitgirard, J. T. Delitz et al., "The Extreme Conditions Beamline P02.2 and the Extreme Conditions Science Infrastructure at Petra III", *J. Synchrotron Rad.* **22** 908–924 (2015).

[11]H. K. Mao, J. Xu and P. M. Bell, "Calibration of the ruby pressure gauge to 800 kbar under quasi-hydrostatic conditions", *J. Geophys. Res.*, **91,** 4673-4676 (1986).

[12]S. Klotz, J-C. Chervin, P. Munsch and G. Le Marchand, "Hydrostatic limits of 11 pressure transmitting media", *J. Phys. D (Appl. Phys.)*, **42,** 075413 (2009).

[13]Agilent (2012) Xcalibur CCD system, CrysAlis Software system.

[14]A. Rothkirch, G. D. Gatta, M. Meyer, S. Merkel, M. Merlini and H-P. Liermann, "Single-crystal diffraction at the Extreme Conditions beamline P02.2: procedure for collecting and analyzing high-pressure single-crystal data", *J. Synchrotron Rad.*, **20,** 711-720 (2013).

[15]G. M. Sheldrick, "SHELX-97. Programs for crystal structure determination and refinement", University of Göttingen, Germany, 1997.

[16]G. M. Sheldrick, "A short history of SHELX", *Acta Cryst.*, **A64,** 112-122 (2008).

[17]A. C. Larson, "Inclusion of secondary extinction in least-squares calculations", *Acta Cryst.*, **23,** 664–665 (1970).

[18]F. D. Murnaghan, "Finite deformations of an elastic solid", *Am. J. Math.*, **49,** 235-260 (1937).

[19]F. Birch, "Finite elastic strain of cubic crystal", *Phys. Rev.*, **71,** 809-824 (1947).

[20]R. J. Angel, "EOS-FIT V5.2. Computer program", www.rossangel.com, 2001, Accessed online 03/01/2017.

[21]R. J. Angel, "Equations of State". Chapter 2 in *High-Temperature and High-Pressure Crystal Chemistry.* Edited by R. M. Hazen and R. T. Downs. *Rev. Mineral. Geochem.* **41** 35–60. Mineralogical Society of America and Geochemical Society, Washington DC, USA, 2000.

[22]G. D. Gatta, N. Rotiroti, M. Fisch and T. Armbruster, "Stability at high pressure, elastic behavior and pressure-induced structural evolution of ''Al_5BO_9'', a mullite-type ceramic material", *Phys. Chem. Minerals*, **37,** 227-236 (2010).

[23]G. D. Gatta, P. Lotti, M. Merlini, H-P. Liermann and M. Fisch, "High-pressure behavior and phase stability of Al_5BO_9, a mullite-type ceramic material", *J. Am. Ceram. Soc.*, **96,** 2583–2592 (2013).

[24]J. Schreuer, B. Hildmann and H. Schneider, "Elastic properties of mullite single crystals up to 1400°C", *J. Am. Ceram. Soc.*, **89,** 1624–1631 (2006).

[25]G. D. Gatta, "Extreme deformation mechanisms in open-framework silicates at high-pressure: Evidence of anomalous inter-tetrahedral angles", *Micropor. Mesopor. Mater.*, **128,** 78–84 (2010).

[26]G. D. Gatta**,** R. J. Angel, J. Zhao, M. Alvaro, N. Rotiroti and M. A. Carpenter, "Phase stability, elastic behavior, and pressure-induced structural evolution of kalsilite: A ceramic material and high-*T*/high-*P* mineral", *Am. Mineral.*, **96,** 1363–1372 (2011).

[27]G. D. Gatta and Y. Lee, "Zeolites at high pressure: A review", *Mineral. Mag.,* **78,** 267-291 (2014).

[28]R. S. Carter, H. Palevsky, V. W. Myers and D. J. Hughes, "Thermal Neutron Absorption Cross Sections of Boron and Gold", *Phys. Rev.*, **92**, 716–721 (1953).

[29]H. Rauch and W. Waschkowski, “Neutron scattering lengths”. In *Neutron Data Booklet.* Edited by A. J. Dianoux and G. Lander. 1-18. First edition. Institute Laue-Langevin, Grenoble, France, 2002.

[30]A. Machiels and R. Lambert, *Handbook on neutron absorber materials for spent nuclear fuel applications*. Electric Power Research Institute, Palo Alto, CA, 2005.

[31]R. F. Barth, A. H. Solloway and R. G. Fairchild, “Boron Neutron Capture Therapy of Cancer”, *Cancer Res.*, **50,** 1061-1070 (1990).

Table 1. Unit-cell constants of londonite at different pressures.

P (GPa)	*V* (Å^3)
0.0001	390.8(2)
1.28(5)	388.8(2)
1.70(5)	387.8(2)
3.05(5)	385.5(2)
3.61(5)	384.0(2)
4.48(5)	382.6(2)
6.50(5)	379.5(2)
8.58(5)	376.7(2)
9.59(5)	375.0(2)
10.50(5)	373.6(2)
12.11(5)	371.6(2)
13.38(5)	369.4(2)
14.41(5)	368.4(2)
15.72(5)	366.6(2)
16.84(5)	365.2(2)
17.81(5)	364.0(2)
18.48(5)	363.1(2)
19.30(5)	361.9(2)
20.24(5)	361.2(2)
21.48(5)	359.4(2)
23.48(5)	357.2(2)
26.16(5)	353.9(2)
16.73(5)*	364.9(2)
4.70(5)*	383.3(2)
1.04(5)*	389.0(2)

** In decompression*

Table 2. Relevant bond distances (Å) and angles (°) at different pressures. Other structural parameters are available in the CIFs (deposited).

P (GPa)	Be-O1	Be-O3 (x3)	O3-Be-O3 (x3)	O3-Be-O1 (x3)	B-O2 (x2)	B-O3 (x2)	O2-B-O3 (x2)	O2-B-O3' (x2)	O3-B-O3	O2-B-O2	Al-O1 (x3)	Al-O2 (x3)	Cs-O3 (x12)
0.0001*	1.553(1)	1.638(1)	112.91(6)	105.77(7)	1.495(1)	1.484(1)	107.89(5)	108.69(5)	112.24(8)	111.48(8)	1.899(1)	1.908(2)	3.235(1)
1.28(5)	1.555(8)	1.634(3)	112.8(2)	105.9(3)	1.493(2)	1.487(2)	107.9(1)	108.9(1)	111.8(2)	111.3(2)	1.904(2)	1.896(3)	3.221(2)
1.70(5)	1.555(8)	1.636(3)	112.8(2)	105.9(2)	1.494(2)	1.483(2)	108.0(1)	108.7(1)	111.8(3)	111.6(2)	1.898(2)	1.893(2)	3.223(2)
3.05(5)	1.560(9)	1.626(4)	112.9(2)	105.8(3)	1.487(3)	1.487(3)	107.8(2)	109.1(2)	111.5(3)	111.6(3)	1.897(3)	1.890(3)	3.206(3)
3.61(5)	1.560(8)	1.625(3)	112.9(2)	105.7(2)	1.488(2)	1.482(2)	107.8(1)	109.1(1)	111.7(2)	111.4(2)	1.895(2)	1.887(3)	3.202(3)
4.48(5)	1.546(9)	1.620(3)	112.8(2)	105.9(3)	1.486(3)	1.482(3)	107.9(1)	109.0(1)	112.0(3)	111.1(3)	1.895(2)	1.886(3)	3.197(3)
6.50(5)	1.551(8)	1.615(3)	112.8(2)	105.9(2)	1.482(2)	1.481(2)	107.7(1)	109.3(1)	111.7(2)	111.3(2)	1.888(2)	1.881(2)	3.182(2)
8.58(5)	1.553(8)	1.613(3)	112.7(2)	106.0(3)	1.482(2)	1.476(3)	107.6(1)	109.5(1)	111.4(3)	111.2(3)	1.885(2)	1.871(3)	3.167(3)
9.59(5)	1.548(8)	1.610(3)	112.6(2)	106.1(3)	1.478(2)	1.477(2)	107.4(1)	109.6(1)	111.2(3)	111.6(3)	1.883(2)	1.869(3)	3.159(3)
10.50(5)	1.540(8)	1.609(3)	112.4(2)	106.3(2)	1.478(2)	1.475(2)	107.5(1)	109.6(1)	111.2(3)	111.5(3)	1.881(2)	1.865(3)	3.153(3)
12.11(5)	1.540(7)	1.608(3)	112.5(2)	106.3(2)	1.476(2)	1.473(2)	107.3(1)	109.8(1)	110.8(2)	111.8(2)	1.879(2)	1.861(2)	3.143(2)
13.38(5)	1.546(7)	1.604(3)	112.7(2)	106.0(2)	1.475(2)	1.470(2)	107.3(1)	109.8(1)	110.8(2)	111.9(2)	1.874(2)	1.856(2)	3.136(2)
14.41(5)	1.540(8)	1.603(3)	112.6(2)	106.1(2)	1.474(2)	1.469(3)	107.3(1)	109.9(1)	110.7(2)	111.7(2)	1.875(2)	1.854(3)	3.131(3)
15.72(5)	1.543(7)	1.599(3)	112.6(2)	106.2(2)	1.473(2)	1.466(2)	107.3(1)	110.0(1)	110.9(2)	111.4(2)	1.870(2)	1.850(2)	3.123(2)
16.84(5)	1.540(6)	1.597(3)	112.7(2)	106.0(2)	1.470(2)	1.463(2)	107.3(1)	109.9(1)	111.0(2)	111.6(2)	1.868(2)	1.850(2)	3.123(2)
17.81(5)	1.550(9)	1.593(4)	112.9(3)	105.7(3)	1.470(3)	1.462(3)	107.1(2)	110.1(1)	110.8(3)	111.6(3)	1.866(3)	1.849(4)	3.114(4)
18.48(5)	1.544(8)	1.597(3)	112.6(2)	106.1(3)	1.470(3)	1.460(3)	107.3(1)	110.0(2)	110.7(3)	111.7(3)	1.862(3)	1.844(3)	3.113(3)
19.30(5)	1.543(8)	1.590(3)	112.7(2)	106.1(3)	1.469(3)	1.461(3)	107.1(1)	110.2(1)	110.8(3)	111.6(3)	1.861(3)	1.843(3)	3.103(3)
20.24(5)	1.548(8)	1.586(3)	112.8(2)	105.9(3)	1.467(3)	1.461(3)	107.0(1)	110.3(1)	110.9(2)	111.5(3)	1.861(2)	1.842(3)	3.099(3)
21.48(5)	1.550(10)	1.588(4)	112.7(3)	106.0(3)	1.469(3)	1.457(3)	107.2(2)	110.1(2)	110.7(3)	111.6(3)	1.854(3)	1.833(3)	3.093(4)
23.48(5)	1.560(11)	1.580(4)	113.0(3)	105.6(3)	1.463(4)	1.457(4)	106.9(2)	110.7(2)	110.5(3)	111.2(3)	1.851(3)	1.839(4)	3.079(4)
26.16(5)	1.553(11)	1.578(5)	113.0(3)	105.7(4)	1.461(4)	1.452(4)	107.0(2)	110.6(2)	110.2(4)	111.5(4)	1.850(4)	1.824(5)	3.069(5)
16.73(5)**	1.545(8)	1.597(3)	112.6(2)	106.1(3)	1.473(3)	1.463(3)	107.1(1)	110.2(1)	110.8(2)	111.5(2)	1.867(2)	1.849(3)	3.113(3)
4.70(5)**	1.546(6)	1.625(3)	112.6(2)	106.1(2)	1.486(2)	1.485(2)	107.7(1)	109.1(1)	111.5(2)	111.9(2)	1.894(2)	1.885(2)	3.198(2)

*Data from Gatta et al.[2], with a = 7.3098(2) Å ; **In decompression.

Figure 1. Two views of the crystal structure of londonite. B-tetrahedra (light grey), Be-tetrahedra (medium grey) and Al-octahedra (dark grey) are shown as solid polyhedra. Cs sites lie at the unit-cell origin.

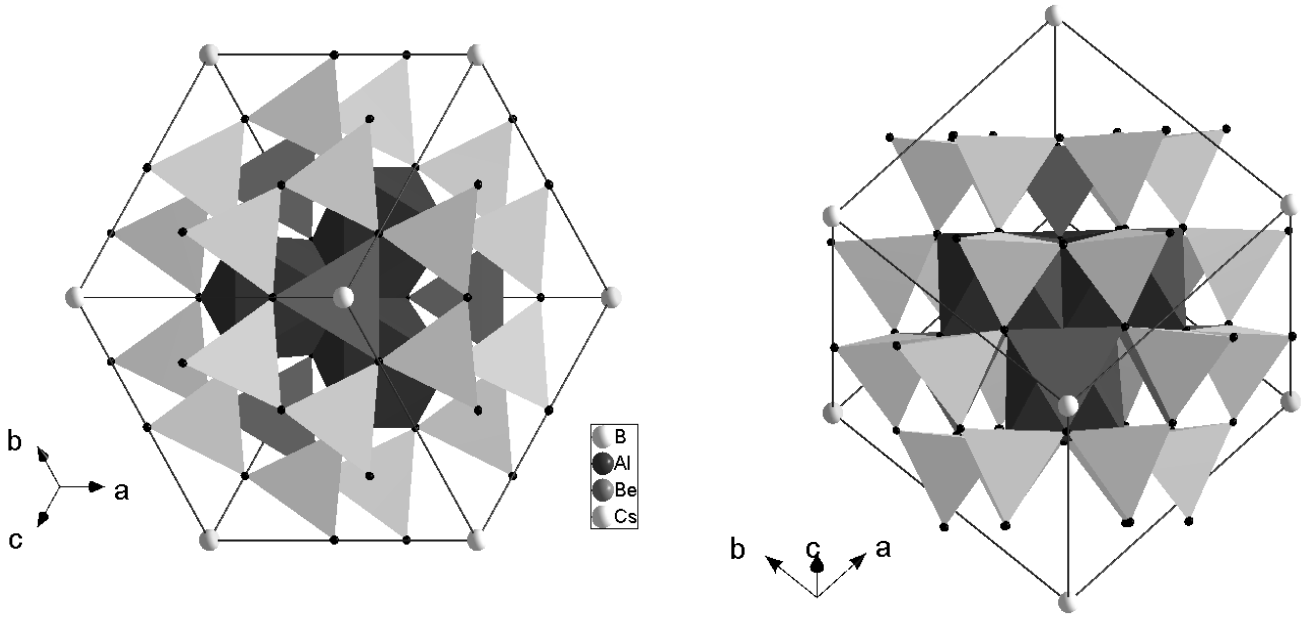

Figure 2. Evolution of the unit-cell volume of londonite with *P* and III-BM-EoS fit (grey symbols: data points in decompression); evolution the Eulerian finite strain *vs.* the normalised pressure plot; confidence-ellipses (referred to the 68.3%, 95.4% and 99.7% confidence-levels) obtained from the least-squares procedure for the III-BM-EoS fit (see text for details).

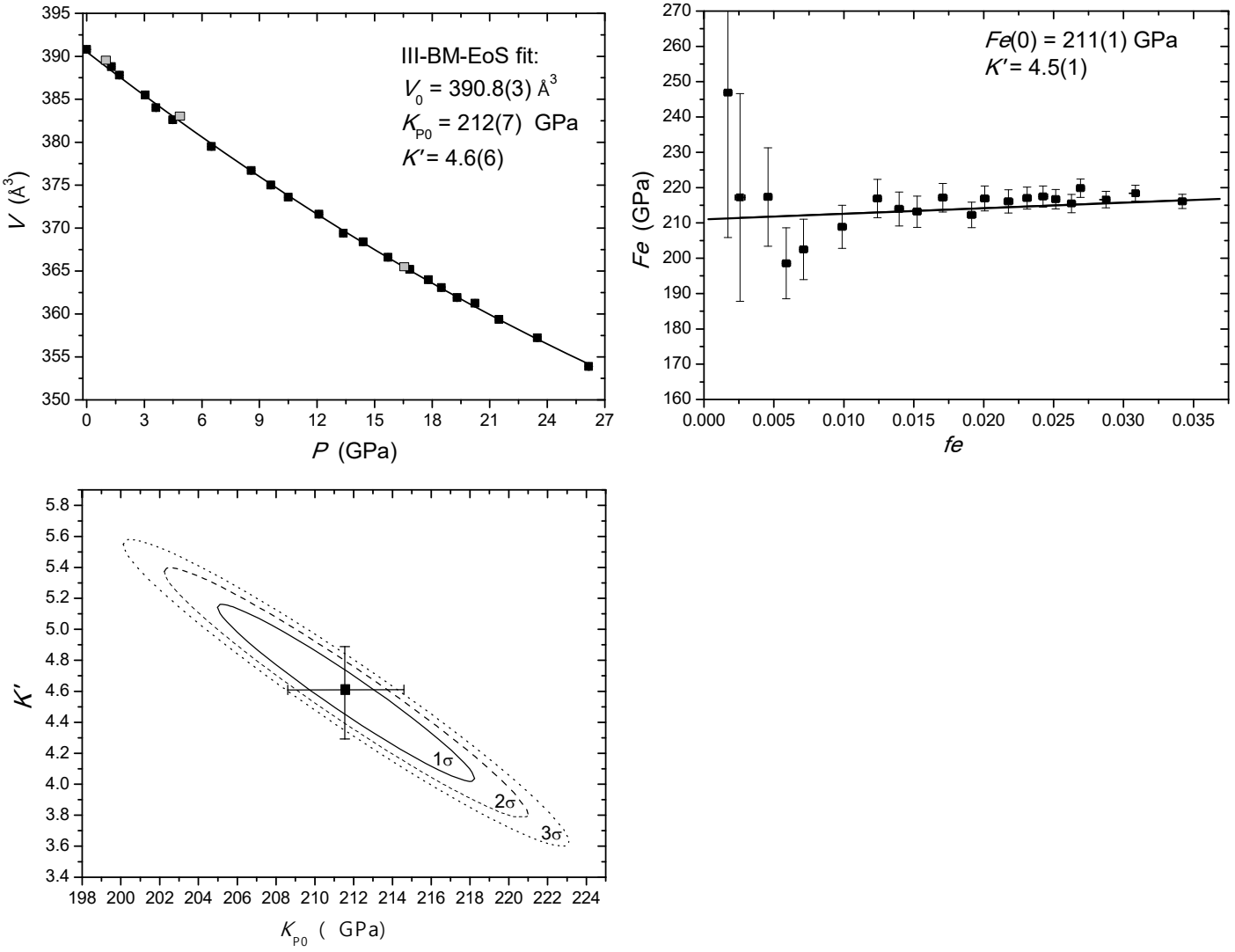

Figure 3. Evolution of some selected bond distances and angles with *P*, listed in Table 2.